Dimensional analysis of Ni-NiO grains at anode/electrolyte interface for SOFC during redox reaction

Bo Liang[1], Silong Zhang[1], Zefang Zhang[2], Biao Lu[1], Shengguo Lu[1], Michaela Kendall[3], Meng Ni[4]

[1] Guangdong Provincial Key Laboratoryof Functional Soft Condensed Matter,School of Materials and Energy,Guangdong University of Technology,Guangzhou, China

[2] Engineering Research Center ofAdvanced Lighting Technology andInstitute for Electric Light Source, FudanUniversity, Shanghai, China

[3] School of Metallurgy and Materials,University of Birmingham, Birmingham,UK

[4] Department of Building and Real Estate,The Hong Kong Polytechnic University,Hong Kong, China

Abstract

Upon reduction and re-oxidization, the interface of a microtubular solid oxide fuel cell (MTSOFC) anode/electrolyte was structurally analyzed using a dual beam focused ion beam/scanning electron microscope (FIB/SEM) and scanning transmission electron microscopy combined with energy dispersive X-ray spectrometer (STEM-EDX). The bulk volume of the dense NiO phase dramatically contracted upon reduction, while the YSZ phases are completely unaffected. No cracks or particle detachment are observed either at the interface of the anode/electrolyte or in the anode backbone. Compared with the initial NiO state (as-prepared), the area of Ni phase contracts by 22.6%-83.7%, depending on the grain size.

1 Introduction

Anode supported MTSOFCs with a thin electrolyte were under intensive research and development in the past decades, because they were designed to operate at temperatures between 650 and 800°C. Despite an active search for alternative materials, the most commonly used anode of a SOFC consists of two phases: (i) electron-conducting nickel and (ii) ion-conducting yttria stabilized zirconia (YSZ). Nickel is usually selected as catalyst due to its very high activity for electrochemical oxidation of hydrogen[1] and reforming of hydrocarbon fuels.[2] These anodes are expected to go through multiple redox cycles during SOFC long-term operation. As long as fuel (H_2, CO, NH_3, or hydrocarbon) is supplied to the anode, NiO is reduced into metallic Ni, while oxidation of the Ni phase occurs if the fuel supply is interrupted (a shutdown, lack of fuel, etc.) or air leaks through the sealing. These reactions resulted in large dimensional grain change between Ni and NiO. This volume change can considerably affect the long-term stability of SOFCs.

Much of the research in redox behavior of Ni/YSZ anodes in the past few years has examined how expansion/contraction affects the porosity, stiffness, three-phase boundaries, and the mechanical stability of the SOFC stack. Ivey et al.[3] studied the redox kinetics of a Ni/YSZ cermet between 450 and 850°C by thermogravimetric analysis (TGA). They mentioned in their study that the bulk volume of a fully dense NiO sample should contract by 40.9% upon reduction and expand by 69.2% upon oxidation. Pihlatie et al.[4] found that Young's moduli of

the anode composites show a linear dependence on porosity before and after reduction, and damage caused by redox cycling degraded the elastic properties of the composites. Faes et al.[5] observed the reduction and oxidation of nickel within Ni/YSZ anode between 300 and 500°C. According to their results, nanopores were formed upon reduction due to a high volume decrease, while nanocrystallites fill up the pores during oxidation. In order to overcome the large dimensional changes of nickel phase, two-step infiltration (both YSZ and polymeric nickel oxides) into a sintered porous YSZ skeleton was presented by Buyukaksoy et al.[6] There was not significant loss in the surface area and porosity, and the reinforced SOFC by two-step infiltration shows a significantly improved performance. Sumi et al.[7] used FIB-SEM to reconstruct the Ni-YSZ anode after redox cycles. It was found that the three phase boundary length decreased from 2.49 μm/μm^3 to 2.39 μm/μm^3 and 2.11 μm/μm^3 after the first and forth cycles respectively. Furthermore, it was also noted that the surface area of the nickel phase increased and these Ni particles became more complicated in shape after redox cycles.

Although important understanding of the redox behavior of NiO-YSZ cermets was developed, how the nickel phase volume varies with particle size, and the redox behaviors of these phases near the anode/electrolyte interface have not been reported up to date. This paper examines a new measure of nickel grain size within the YSZ network based on a FIB/SEM thinning TEM lamella which overcomes the difficulties of exactly tracking the position of nickel grains during redox testing used in other measures. In the second section of this study, after an introduction of how to thin down the as-observed TEM lamella, various effects were investigated: firstly, the effect of hydrogen processing for the anode/electrolyte interface; then the porosity, pore size, shrinkage, and three phase boundary of this region were studied; lastly, the microstructure of the reduced and re-oxidized interface were compared.

2 Experimental Section

2.1 Cell fabrication

The fabrication process of a single cell can be divided into three steps. (i) Anode tubes were made by mixing NiO powder (Ningbo SOFCMAN Energy Technology, Ningbo, China), Y_2O_3-stabilized ZrO_2 (YSZ) (Ningbo SOFCMAN Energy Technology), 30 vol% of pore former (PMMA beads, D50=3 μm), and binder. The ratio of YSZ: NiO was 40:60 (wt%). Then, anode tubes were extruded from a metal mold using a piston cylinder type extruder (Xinlong Machinery Factory). An extremely thin YSZ electrolyte about 5 μm in thickness was formed after co-sintering the anode/electrolyte at 1350°C for 1 hour. The electrolyte was fabricated by dip-coating. The electrolyte slurry consisted of YSZ powder, toluene, alcohol, binder (Polyvinyl Butyral, PVB), and dispersant. During the dip-coating process, the substrate (anode tube) remained inside the slurry for 10 seconds, then was pulled up with a speed of 1 mm/s. (ii) Following further sintering, the anode/electrolyte (co-sintered at 1380°C) was again dip-coated in a GDC slurry and sintered at 1150°C for 1 hour. The thickness of the GDC interlayer was about 1 μm following sintering.

2.2 FIB thinning, redox testing of the interface, and electron microscope observation

For eroding the electrolyte/interlayer interface, a FIB/SEM dual-beam instrument (FEI, Hillsboro, OR) was used. The TEM lamella of the NiO-YSZ/YSZ/GDC/carbon interfaces was extracted using a lift-out technique with a micromanipulator within the FIB/SEM chamber. The lamella was glued on a copper grid by deposited carbon. Thinning down of the TEM sample to about 150 nm was achieved with an ion beam at accelerated voltage of 5 kV. The redox cycling of the copper grid supported TEM lamella was carried out by switching dry diluted hydrogen

(15% H_2 and 85% Ar) to air. The temperature for reduction and oxidation was 800°C with an exposure time of 4 hours. Four-point conductivity measurements are performed for Ni-YSZ anode conductivity using diluted hydrogen (15% H_2 and 85% Ar) at 600 and 800°C. The tubular anodes were placed in an alumina tube, and four silver wires were attached with the conductivity measurement probes. The detailed microstructural features of reduced TEM lamella were then examined by TEM (JEM-2100F operated at 200 kV; JEOL, Tokyo, Japan) equipped with an EDX detector. To investigate the chemical composition and spatial distribution, the EDX investigation was performed in the dark-field scanning TEM (DF-STEM) mode with 1 nm resolution. Because the copper grid would become brittle at high temperatures, the microstructural features of oxidized lamella was observed by SEM (HITACHI SU8010; HITACHI, Tokyo, Japan) equipped with an EDX detector (IXRF System).

3 Results and Discussion

In order to protect the upper surface, a protecting carbon layer (~1 μm in thickness) was coated on the GDC interlayer using ion-beam induced deposition. Figure **1** shows the FIB eroding process, which includes several steps from a TEM lamella cutting, through the specimen lift-out and transfer, to localized erosion of the lamella. When fabricating the TEM specimen, the ion beam scanning (frontward and backward) started 2 μm away from both the edges of carbon deposition. The ion beam (beam current: 0.8-2.9 nA) gradually cut two trenches on each side of the lamella, a shallow one and a sufficiently deep one, leaving behind a thinned lamella (~1 μm) supported by bulk material. A thickness of 1 μm is kept to avoid a strong bending of the sample. Then, a tungsten probe was used for the TEM specimen lift-out and transfer. Figure **1**(C) shows the top view of wedge shaped lamella. The left side of the sample was fixed to the copper grid using carbon injection, while the right hand side of the lamella was thinned to 150 nm. Thickness values were measured with a layer probe. As the lamella thickness decreased, the ion beam current was progressively decreased, from 1 nA to 200 pA. The sample preparing ended with a cleaning step, which was done using a 1 kV ion beam. In Figure **1**(D), it is seen that the interfaces below carbon deposition are well-protected in the fine milling area.

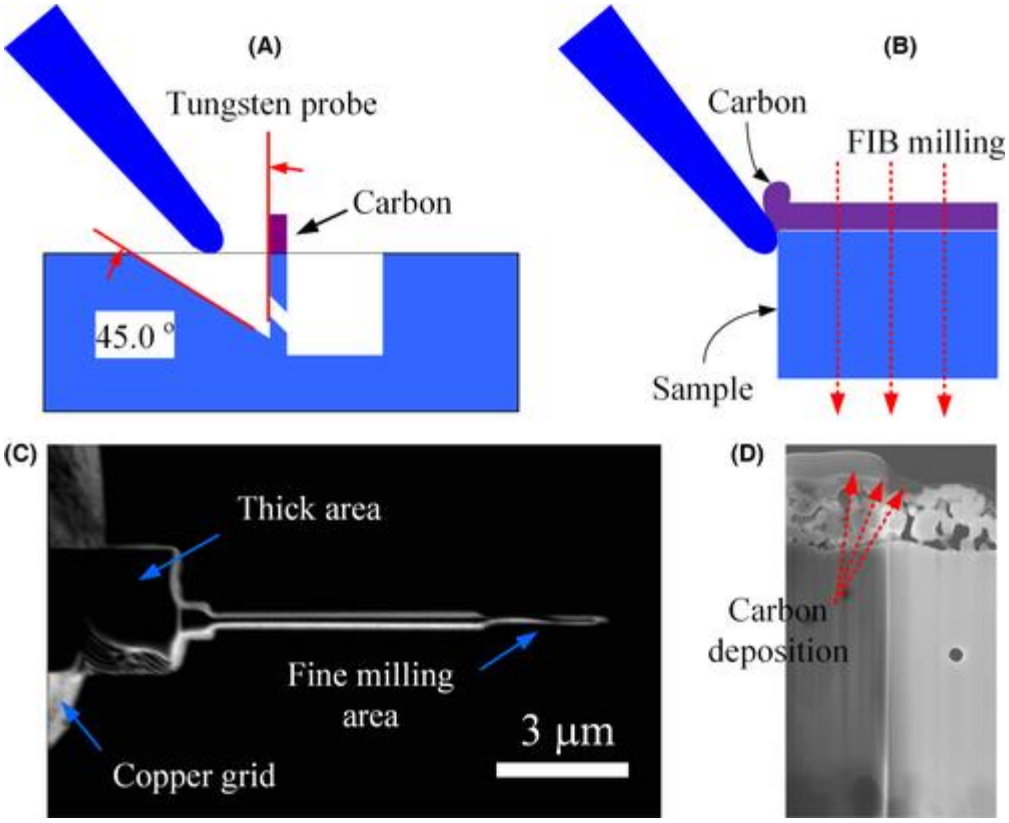

Figure 1

(A) and (B) show the principle sketch of the FIB milling process and the TEM sample transfer process, respectively; (C) shows the top view of the NiO-YSZ/YSZ interface mounted on TEM copper grid; (D) shows the carbon deposition for protecting the TEM specimen below it

Figure **2** compare the STEM-DF images of the anode/electrolyte interface before and after H_2 reducing respectively. As can be seen in Figure **2**(A), relatively sharp grain boundaries are easily distinguishable in the DF image of the prepared interface (oxidized). Different composite elements corresponded to different contrasts in the image. The microstructures of the interface suggest that the electrolyte was highly dense, and grain size of both NiO and YSZ phases were roughly 1 μm. Figure **2**(B) clearly shows the distribution of reduced Ni and unaffected YSZ of the TEM lamella. The bulk volume of the dense NiO phase clearly contracts upon reduction, while the YSZ phase was almost completely unaffected by the H_2 reduction process. After being heated to 800°C in 15% H_2 for 4 hours, the porosity of the anode was increased, and the YSZ electrolyte kept quite stable. An aggregate-type morphology of Ni grains can also be observed by STEM-DF. This core (Ni)—shell (YSZ) structure was reported by Waldbillig et al.[8] Figure **3** demonstrates the STEM-EDX map-scanning results of the Ni-YSZ/YSZ interface after reduction by hydrogen, and confirms that it is a Ni-YSZ anode supported Zr-based electrolyte. The existence of oxygen in the anode provides evidence that the YSZ is very stable when reduced. Although it is known that ZrO_2 basically remains unaffected by reduction in hydrogen up to temperatures of 1773 K,[9] it is worth noting that YSZ does not show any noticeable morphological changes at 1073 K for 2 hours of hydrogen reduction. Furthermore, no cracks or particle detachment are observed either at the interface of the anode/electrolyte or in the anode backbone. A few Ni nano-particles, labeled by white arrows, decorate the inner surface of the large pore, but the exact diffusion mechanism still remains unclear from these images.

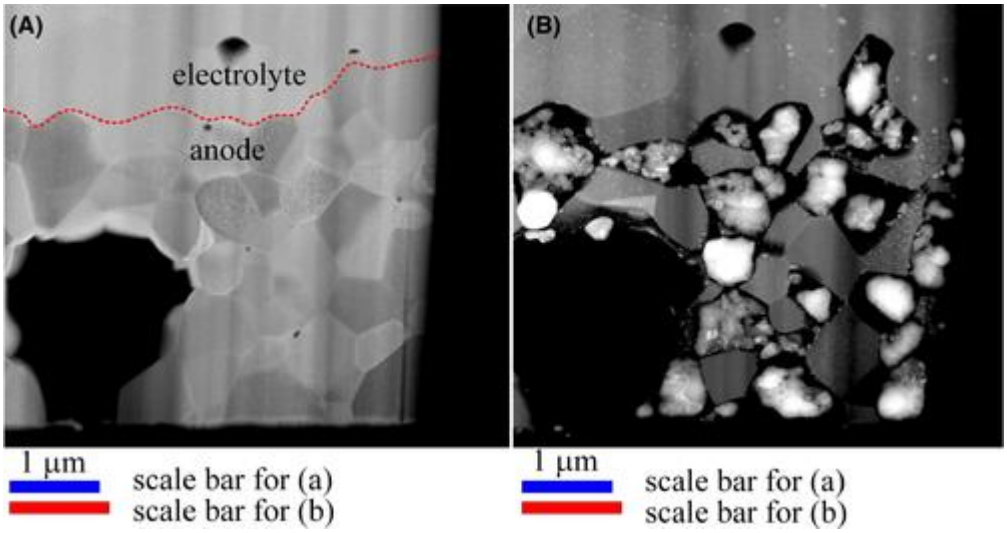

Figure 2

STEM-DF images for the interface of anode/electrolyte: (A) prepared by FIB; (B) reduced microstructure

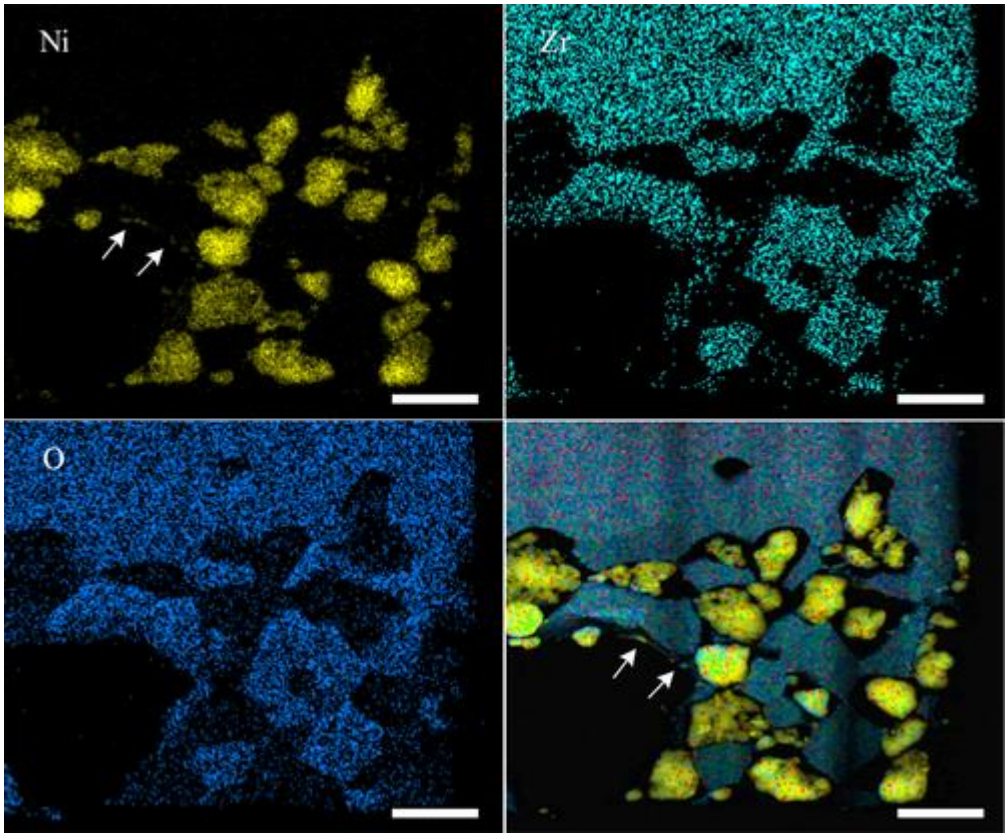

Figure 3

EDS elemental map of the anode/electrolyte interface after H2 reduction, constructed by superimposing Zr, Ni, and O maps

Figure **4**(A) shows the high resolution STEM-DF image of Ni and YSZ phases along the anode/electrolyte interface. The reduced anode exhibits significantly smaller Ni particles, and the presence of tiny pores within the Ni grains can also be seen. Some Ni particles are discrete

particulate material, and some Ni grains agglomerate, minimizing surface energy. The pore size distribution is calculated based on the chord length which can be drawn in the pore space surrounded by these Ni grains. The size of these pores ranges from a few nm to 100 nm, and the most probable value of diameter is about 8 nm. The electrochemical reactions are believed to occur within a small depth (from several μm to a few tens of μm) of the electrolyte/anode interface,[10-12] which is known as the electrochemically active thickness (EAT). Therefore, only TPBs within this region are useful for electrochemical reactions and TPBs out of this region are considered not to contribute to electrochemical reactions. As shown in Figure **4**(B), the TPBs are represented by the yellow lines, and the value is about 7.8 $\mu m/\mu m^3$. This value is larger than those reported in the literature (between 1 and 6 μm^{-2}).[13-28] For example, the TPB value is about 2 μm^{-2} when a Ni-YSZ anode was reduced at 950°C.[20] Two possible factors can contribute to the increased length in TPB: first, the reduction temperature is 800°C, lower than 950°C; second, the current TPB value is measured for a small TEM sample, many nano-sized Ni particles are tightly attached to the YSZ grains, the boundaries of "Ni phase" and "YSZ phase" are easy to distinguish in high resolution DF-STEM. Furthermore, the value of shrinkage ranged from 22.6% to 83.7% in area. If those Ni particles are round in shape in the literature, the mean value of this study reaches 53.3%, which is larger than 66.6% (shrink 40.9% in volume) reported by Waldbillig et al.[3] and 67.7% (shrink 42% in volume)reported by Timurkutluk and Mat[29] respectively. Figure **5** shows the difference in the electrical conductivity of Ni-YSZ anode tubes following reduction at 600 and 800°C. Initial electrical conductivities were 982 S/cm (after the second reduction) and 562 S/cm at 600 and 800°C respectively. These values then dropped to 862 and 353 S/cm after 8 redox cycles. The linear trends from the second to the eighth cycle are interpreted as typical redox behavior. These results demonstrate that high reducing temperature results in the high shrinkage of Ni phase and an associated drop in electrical conductivity.

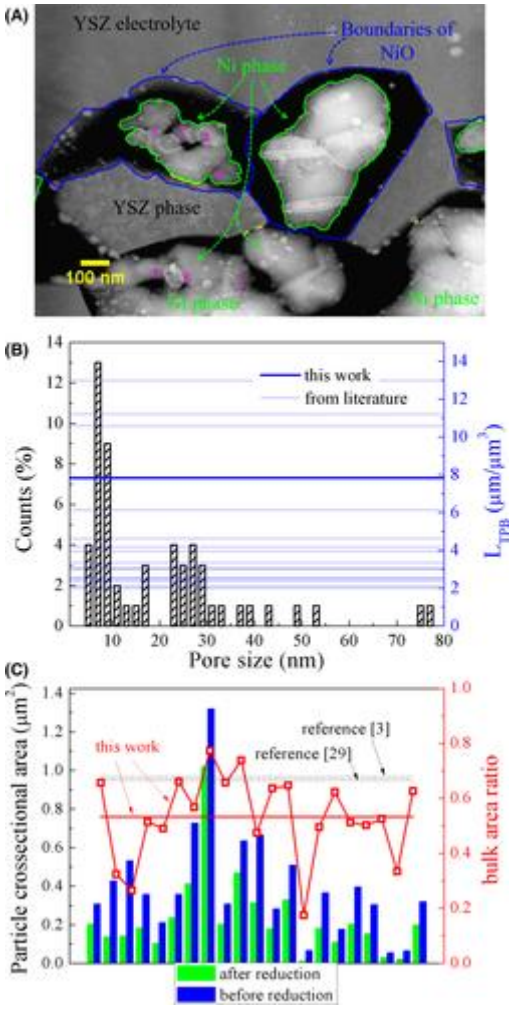

Figure 4

(A) HR-STEM-DF image for the interface of anode/electrolyte. The blue lines show the outer boundary of the NiO phase, the green lines show the Ni grains after reducing, and the yellow color is the contact line of TPB; (B) the pore size distribution within the Ni cluster and TPB length of region shown in Figure 2(B); (C) comparison of the cross-sectional areas of the Ni upon reduction and the initial NiO phase, and the normalized ratio of them

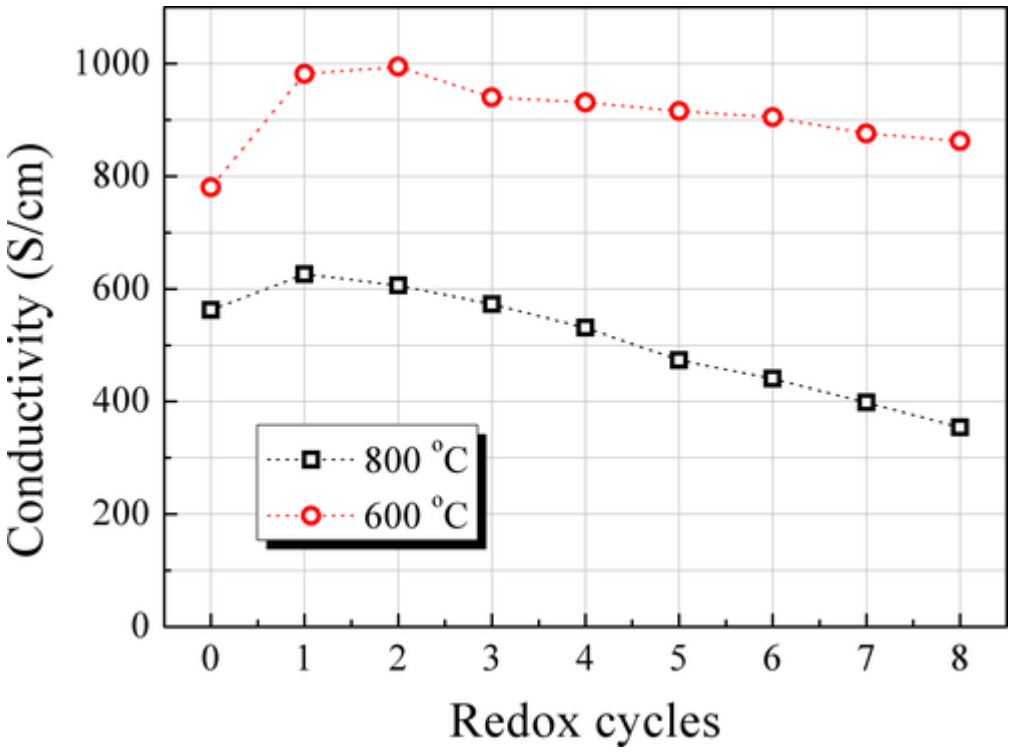

Figure 5

Evolution of the electrical conductivity of anode during eight cycles at 600 and 800°C

Interestingly, the microstructure of most NiO particles cannot be restored upon re-oxidation (see Figure **6**[A]). It was also found that the re-oxidation strain did not cause electrolyte cracking during operation (800°C for 4 hours). The magnitude of expansion, in this work, depends strongly on the actual grain size. It is worthy to note that the volumes of those small grains (labeled by the yellow arrows) were restored in this study. Considering this observation, a lower size distribution of NiO particles in the anode could result in lower electronic conductivity after reduction and significant structural changes in anode microstructure after re-oxidation. As shown in Figure **6**(B), the initial reduction leads to a contraction of approximately 50% in area, while the re-oxidation expansion reaches to 65% of the original value of NiO phase (as-prepared). Assuming the Ni particles are spherical, the oxidation-induced expansion is estimated to about 48.2% in volume. It is smaller than 69.9% reported by Sarantaridis and Atkinson [30] based on the molar volumes of Ni and NiO. This expansion difference could be caused by partial oxidation of the Ni phase at 800°C. Figure **6**(C) shows the shrinkage ratio of various NiO particles after 1st reducing and 1st reoxidation. Since smaller Ni particle may be fully oxidized while larger one may be partially oxidized during the oxidation process, it was found that the oxidation-induced expansion of the Ni particles (labeled by 1, 2 and 3) is larger than that of those bulky grains. As is well-known, the EAT of anode side is less than 10 μm (V_{cell}=0.8 V, operated at 1073 K).[12] Any changing in the mean particle radius of Ni closed to electrolyte could greatly affect EAT of the cell and its performance. So, when designing an SOFC anode/electrolyte, to use very small NiO particles is not well suggested according to the results in this study as well as in the literature[12] (see the figure 10 in it).

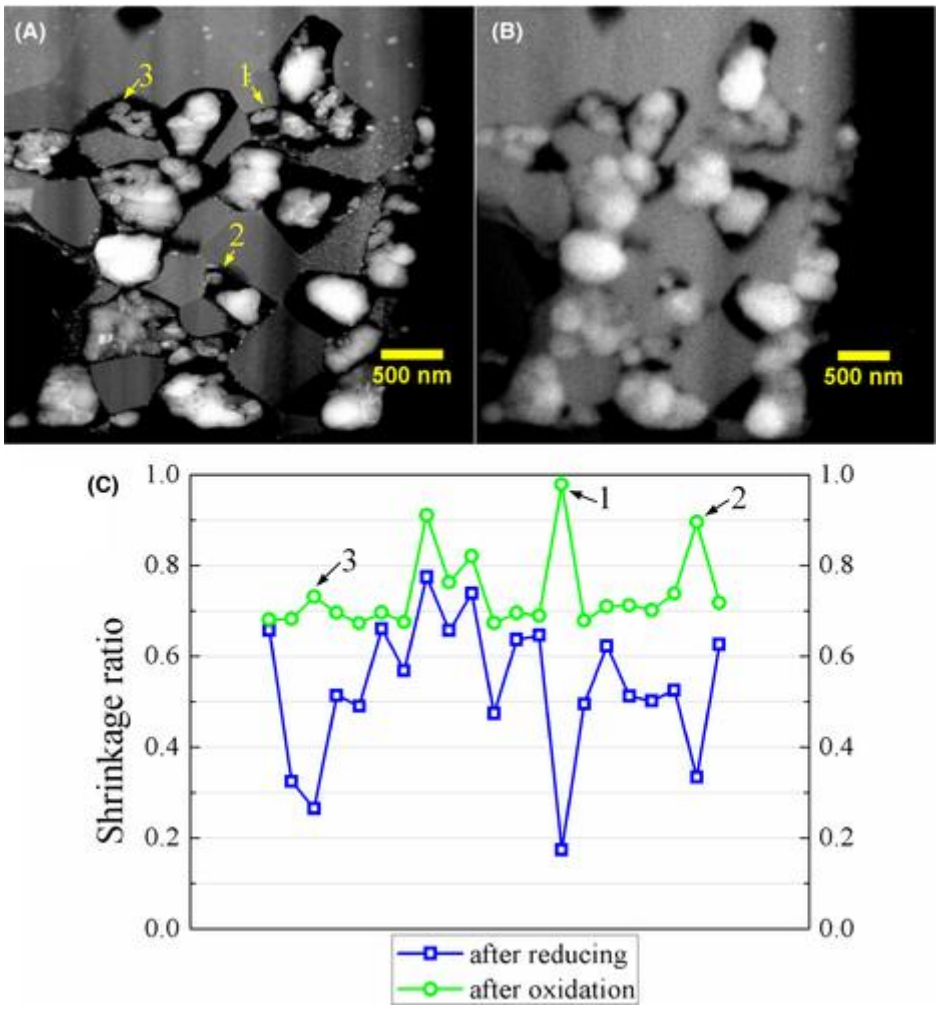

Figure 6

(A) STEM-DF images for the interface of anode/electrolyte after H2 reducing; and (B) SEM image of the interface upon re-oxidization; (C) the shrinkage ratio of various NiO particles closed to the electrolyte

4 Conclusion

This paper studied the dimensional changes of Ni-NiO grains at anode/electrolyte interface of an SOFC, during hydrogen processing. TEM and SEM were used to characterize the microstructure of the prepared, reduced, and re-oxidized samples. Reduction at 800°C resulted in Ni grain contraction of 22.6%-83.7% in area, depending on the grain size, while the YSZ phase was almost completely unaffected. This value is higher than the results of Timurkutluk and Mat[29] and Waldbillig et al.[3] When re-oxidized at the same temperature, most of the expanding metallic nickel can no longer occupy the same original void. Small grains expanded more than those coarse ones, with some grains even restored to their initial volume state. The detailed dimensional results from this anode/electrolyte interface upon reduction/re-oxidization could provide useful parameters for a numerical simulation, and offer a potential mechanistic explanation for changes in conductivity. Further analyses for different PO_2 and kinetic studies with different temperatures for a zirconia anode supported ceria electrolyte interface will be conducted to expand the study.

Acknowledgments

This work was supported by the Start-up funding of Guangdong University of Technology (No. 220413118) and the Innovation Program of under the Support of the Science and Technology Bureau in Foshan (No. 20151T100051).

References

- 1. Jaksic JM, Ristic NM, Krstajic NV, Jaksic MM. Electrocatalysis for hydrogen electrode reactions in the light of fermi dynamics and structural bonding FACTORS—I. Individual electrocatalytic properties of transition metals. *Int J Hydrogen Energy*. 1998; **23**: 1121- 1156.

- 2. Rostrup-Nielsen JR. Activity of nickel catalysts for steam reforming of hydrocarbons. *J Catal*. 1973; **31**: 173- 199.
- 3. Waldbillig D, Wood A, Ivey DG. Thermal analysis of the cyclic reduction and oxidation behaviour of SOFC anodes. *Solid State Ionics*. 2005; **176**: 847- 859.
- 4. Pihlatie M, Kaiser A, Mogensen M. Mechanical properties of NiO/Ni–YSZ composites depending on temperature, porosity and redox cycling. *J Eur Ceram Soc*. 2009; **29**: 1657- 1664.
- 5. Faes A, Jeangros Q, Wagner JB, et al. In situ reduction and oxidation of nickel from solid oxide fuel cells in a transmission electron microscope. *ECS Trans*. 2009; **25**: 1985- 1992.
- 6. Buyukaksoy A, Petrovsky V, Dogan F. Optimization of redox stable Ni-YSZ anodes for SOFCs by two-step infiltration. *J Electrochem Soc*. 2012; **159**: F841- F848.
- 7. Sumi H, Kishida R, Kim J-Y, Muroyama H, Matsui T, Eguchi K. Correlation between microstructural and electrochemical characteristics during redox cycles for Ni–YSZ anode of SOFCs. *J Electrochem Soc*. 2010; **157**: B1747- B1752.
- 8. Waldbillig D, Wood A, Ivey DG. Electrochemical and microstructural characterization of the redox tolerance of solid oxide fuel cell anodes. *J Power Sources*. 2005; **145**: 206- 215.
- 9. Hoang DL, Lieske H. Effect of hydrogen treatments on ZrO_2 and Pt/ZrO_2 catalysts. *Catal Lett*. 1994; **27**: 33- 42.
- 10. Hussain MM, Li X, Dincer I. Mathematical modeling of planar solid oxide fuel cells. *J Power Sources*. 2006; **161**: 1012- 1022.
- 11. Williford RE, Chick LA, Maupin GD, Simner SP, Stevenson JW. Diffusion limitations in the porous anodes of SOFCs. *J Electrochem Soc*. 2003; **150**: A1067- A1072.
- 12. Zheng K, Li L, Ni M. Investigation of the electrochemical active thickness of solid oxide fuel cell anode. *Int J Hydrogen Energy*. 2014; **39**: 12904- 12912.

- 13. Cronin JS, Wilson JR, Barnett SA. Impact of pore microstructure evolution on polarization resistance of Ni-Yttria-stabilized zirconia fuel cell anodes. *J Power Sources*. 2011; **196**: 2640- 2643.

- 14. Jiao Z, Lee G, Shikazono N, Kasagi N. Quantitative study on the correlation between solid oxide fuel cell Ni-YSZ composite anode performance and sintering temperature based on three-dimensional reconstruction. *J Electrochem Soc*. 2012; **159**: F278- F286.

- 15. Kanno D, Shikazono N, Takagi N, Matsuzaki K, Kasagi N. Evaluation of SOFC anode polarization simulation using three-dimensional microstructures reconstructed by FIB tomography. *Electrochim Acta*. 2011; **56**: 4015- 4021.

- 16. Karen Chen-Wiegart Y-c, Cronin JS, Yuan Q, Yakal-Kremski KJ, Barnett SA, Wang J. 3D non-destructive morphological analysis of a solid oxide fuel cell anode using full-field X-ray nano-tomography. *J Power Sources*. 2012; **218**: 348- 351.

- 17. Kishimoto M, Iwai H, Saito M, Yoshida H. Quantitative evaluation of solid oxide fuel cell porous anode microstructure based on focused ion beam and scanning electron microscope technique and prediction of anode overpotentials. *J Power Sources*. 2011; **196**: 4555- 4563.

- 18. Kubota M, Okanishi T, Muroyama H, Matsui T, Eguchi K. Microstructural evolution of Ni–YSZ cermet anode under thermal cycles with redox treatments. *J Electrochem Soc*. 2015; **162**: F380- F386.

- 19. Matsui T, Kishida R, Muroyama H, Eguchi K. Comparative study on performance stability of Ni–oxide cermet anodes under humidified atmospheres in solid oxide fuel cells. *J Electrochem Soc*. 2012; **159**: F456- F460.

- 20. Pecho O, Mai A, Münch B, Hocker T, Flatt R, Holzer L. 3D microstructure effects in Ni-YSZ anodes: influence of TPB lengths on the electrochemical performance. *Materials*. 2015; **8**: 5370.

- 21. Shearing PR, Cai Q, Golbert JI, Yufit V, Adjiman CS, Brandon NP. Microstructural analysis of a solid oxide fuel cell anode using focused ion beam techniques coupled with electrochemical simulation. *J Power Sources*. 2010; **195**: 4804- 4810.

- 22. Shearing PR, Golbert J, Chater RJ, Brandon NP. 3D reconstruction of SOFC anodes using a focused ion beam lift-out technique. *Chem Eng Sci*. 2009; **64**: 3928- 3933.

- 23. Shikazono N, Kanno D, Matsuzaki K, Teshima H, Sumino S, Kasagi N. Numerical assessment of SOFC anode polarization based on three-dimensional model microstructure reconstructed from FIB-SEM images. *J Electrochem Soc*. 2010; **157**: B665- B672.

- 24. Usseglio-Viretta F, Laurencin J, Delette G, Villanova J, Cloetens P, Leguillon D. Quantitative microstructure characterization of a Ni–YSZ bi-layer coupled with simulated electrode polarisation. *J Power Sources*. 2014; **256**: 394- 403.

- 25. Vivet N, Chupin S, Estrade E, et al. Effect of Ni content in SOFC Ni-YSZ cermets: a three-dimensional study by FIB-SEM tomography. *J Power Sources*. 2011; **196**: 9989- 9997.
- 26. Wang X, Atkinson A. Modeling microstructure evolution of Ni cermet using a cellular automaton approach. *J Electrochem Soc*. 2014; **161**: F605- F614.
- 27. Wilson JR, Cronin JS, Barnett SA. Linking the microstructure, performance and durability of Ni-yttria-stabilized zirconia solid oxide fuel cell anodes using three-dimensional focused ion beam–scanning electron microscopy imaging. *Scripta Mater*. 2011; **65**: 67- 72.
- 28. Wilson JR, Gameiro M, Mischaikow K, Kalies W, Voorhees PW, Barnett SA. Three-dimensional analysis of solid oxide fuel cell Ni-YSZ anode interconnectivity. *Microsc Microanal*. 2009; **15**: 71- 77.
- 29. Timurkutluk B, Mat MD. Effects of anode fabrication parameters on the performance and redox behavior of solid oxide fuel cells. *J Power Sources*. 2014; **258**: 108- 116.
- 30. Sarantaridis D, Atkinson A. Redox cycling of Ni-based solid oxide fuel cell anodes: a review. *Fuel Cells*. 2007; **7**: 246- 258.